Poincaré plot interpretation using a physiological model of HRV based on a network of oscillators

MICHAEL BRENNAN,[1] MARIMUTHU PALANISWAMI,[1] AND PETER KAMEN[2]
[1]*Department of Electrical and Electronic Engineering, University of Melbourne, Parkville, Victoria
3010; and* [2]*Department of Cardiology, Austin Hospital, Melbourne, Victoria 3084, Australia*

Brennan, Michael, Marimuthu Palaniswami, and Peter Kamen. Poincaré plot interpretation using a physiological model of HRV based on a network of oscillators. *Am J Physiol Heart Circ Physiol* 283: H1873–H1886, 2002; 10.1152/ajpheart.00405.2000.—In this paper, we develop a physiological oscillator model of which the output mimics the shape of the R-R interval Poincaré plot. To validate the model, simulations of various nervous conditions are compared with heart rate variability (HRV) data obtained from subjects under each prescribed condition. For a variety of sympathovagal balances, our model generates Poincaré plots that undergo alterations strongly resembling those of actual R-R intervals. By exploiting the oscillator basis of our model, we detail the way that low- and high-frequency modulation of the sinus node translates into R-R interval Poincaré plot shape by way of simulations and analytic results. With the use of our model, we establish that the length and width of a Poincaré plot are a weighted combination of low- and high-frequency power. This provides a theoretical link between frequency-domain spectral analysis techniques and time-domain Poincaré plot analysis. We ascertain the degree to which these principles apply to real R-R intervals by testing the mathematical relationships on a set of data and establish that the principles are clearly evident in actual HRV records.

heart rate variability; quantitative beat-to-beat analysis

THE STUDY OF HEART RATE variability (HRV) centers on the analysis of beat-to-beat fluctuations in heart rate. The series of time intervals between heartbeats, referred to as R-R intervals, are measured over a period of anywhere from 10 min to 24 h (15). Attention has focused on HRV as a method of quantifying cardiac autonomic function. In this study, we present new results in developing a novel mathematical model that describes the interactions between the sympathetic and the parasympathetic nervous systems and heart rate fluctuations over a short-term period of 5–10 min. Whereas our model is based on standard and already accepted physiological principles, the mathematical formulation permits in-depth numerical and analytic investigations yielding valuable insight into clinical R-R interval analysis techniques.

Standard analysis techniques commonly estimate the levels of sympathetic and parasympathetic activity from the variability in the R-R intervals. Our attention has focused on two specific HRV analysis techniques. The first is the frequency domain spectral analysis of R-R intervals (2, 4, 6, 14, 20). R-R interval Poincaré plot analysis is the second technique, which is a newer nonlinear method (8–10, 21, 22). To date, R-R interval Poincaré plot analysis has not been clearly related to a physiological model of HRV. The main objective of our model is to provide insight into the significance of Poincaré plot morphology and not to accurately reproduce the complex autonomic activity of any particular individual.

Our model emulates the differing varieties of Poincaré plot patterns seen in subjects over a range of sympathovagal balances. In addition, the model provides a unique link between spectral analysis techniques and the emerging analysis techniques that rely on the shape and/or other morphological properties of the Poincaré plot. Analytic results on the "lengths" and "widths" of the Poincaré plots generated by our model are developed. Simulations are employed to confirm the analytic results on the model. However, the model does not necessarily represent the full range of autonomic activity. Therefore, to evaluate the validity and scope of the model and analysis, we provide results by using a set of data from actual subjects.

GLOSSARY

Model

HR	Mean heart rate, Hz
t	Time, s
k	Beat number
t_k	Time of kth beat, s
$\bar{I}$	Mean interbeat interval, s
C_s	Sympathetic coupling constant, Hz
C_p	Parasympathetic coupling constant, Hz
ω_s	Frequency of sympathetic modulation, rad/s
ω_p	Frequency of parasympathetic modulation, rad/s
$s(t)$	Sympathetic activation

$p(t)$ Parasympathetic activation
$m(t)$ Modulation function, Hz
$x(t)$ IPFM output spike train, Hz
$y(t)$ IPFM integration process output

Analysis

N Number of sinusoids
C_n Coupling constant for sinusoid n, Hz
ϕ_n Phase of sinusoid n, radians
δ_k Deviation time of beat k from regular spike train, s
ω_n Frequency of sinusoid n, rad/s
RR_k Interbeat interval, s
ΔRR_k Delta interbeat interval, s
L Length of Poincaré plot, s
W Width of Poincaré plot, s

HRV indexes

LF   Low-frequency power, $1/s^2$
HF   High-frequency power, $1/s^2$
SDRR   Standard deviation of interbeat intervals, s
SDSD   Standard deviation of successive differences of interbeat intervals, s

HRV ANALYSIS

It is well known that perturbations to autonomic activity, such as respiratory sinus arrhythmia and vasomotor oscillations, cause corresponding fluctuations in heart rate (2, 17). HRV analysis seeks to determine the autonomic activity from heart rate variability. Spectral analysis is the standard technique used to determine the presence of respiratory sinus arrhythmia and vasomotor oscillations (17, 18). This is accomplished by dividing the spectrum into low- (0.04–0.15 Hz) and high- (0.15–0.4 Hz) frequency bands, known as the LF and HF bands, effectively distin-

guishing between rapid respiratory modulator activity and slow vasomotor modulation of heart rate (see Fig. 1*A*). HF power is supposedly a pure measure of parasympathetic activity, and LF power is reflective of sympathetic modulation and parasympathetic tone, although it is sometimes considered to reflect sympathetic tone (6). In this study, spectral estimates are given by the autoregressive parametric technique by using the modified covariance method (12) for the smooth spectrum and easy identification of the spectral peaks.

The Poincaré plot is a scatterplot of the current R-R interval plotted against the preceding R-R interval. Poincaré plot analysis is a quantitative visual technique, whereby the shape of the plot is categorized into functional classes (21, 22). The plot provides summary information as well as detailed beat-to-beat information on the behavior of the heart (9). Points above the line of identity indicate R-R intervals that are longer than the preceding R-R interval, and points below the line of identity indicate a shorter R-R interval than the previous. Accordingly, the dispersion of points perpendicular to the line of identity (the "width") reflects the level of short-term variability. This dispersion can be quantified by the standard deviation of the distances the points lie from the line of identity. This measure is equivalent to the standard deviation of the successive differences of the R-R intervals [standard deviation of successive differences (SDSD) or root-mean-square of successive differences (RMSSD)] (10). The standard deviation of points along the line of identity (the "length") reflects the standard deviation of the R-R intervals (SDRR). Figure 1*B* details these quantitative measures of Poincaré plot shape. Poincaré plots appear under different names in the literature: scatter plots, first return maps, and Lorenz plots being prominent
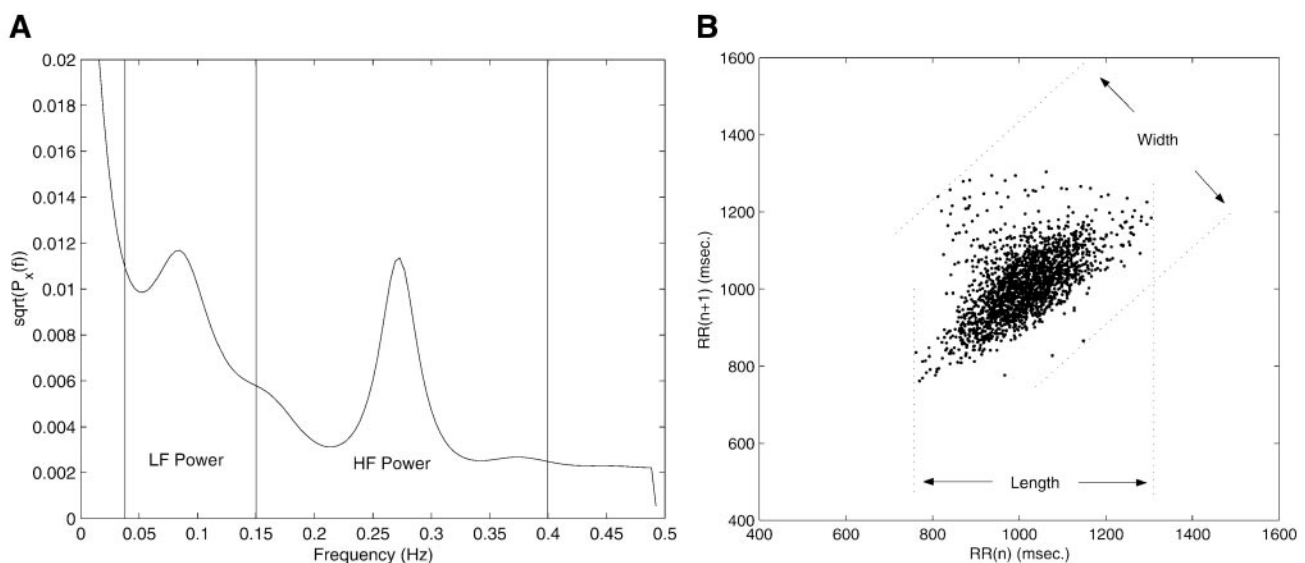

Fig. 1. *A*: heart reat variability (HRV) spectrum. Respiratory component near 0.3 Hz and the vasomotor component near 0.1 Hz are clearly present. HF, high frequency; LF, low frequency. *B*: Poincaré plot of the same data. Length and width are shown graphically on plot.
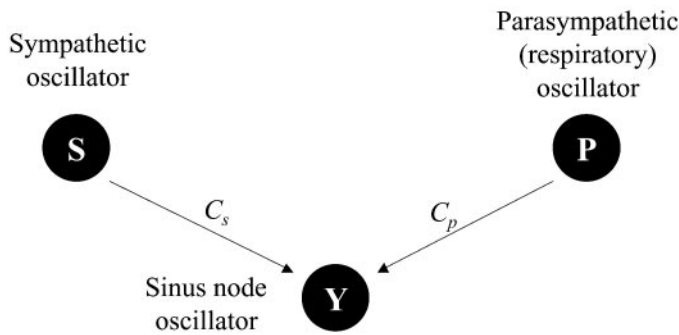
Fig. 2. Three coupled oscillators representing the cardiac control system. C_s, sympathetic coupling constant; C_p, parasympathetic coupling constant.

terms. A distinct advantage of Poincaré plots is their ability to identify beat-to-beat cycles and patterns in data that are difficult to identify with spectral analysis (21, 22).

PHYSIOLOGICAL HRV MODEL BASED ON INTERACTING OSCILLATORS

In this section, we develop a model by using a coupled network of oscillators, each representing a specific facet of the baroreflex and autonomic nervous system. The architecture of the network and the coupling are shown in Fig. 2. The coupling constants C_s and C_p denote the level at which the corresponding oscillator modulates the sinus node oscillator, where s is sympathetic and p is parasympathetic. For the purpose of clarity, we define the respiratory oscillator as the parasympathetic oscillator.

Sympathetic oscillator. The sympathetic oscillator (s) represents the combined LF power of the HRV spectrum, which includes vasomotor activity. It is governed by *Eq. 1*

$$s = \sin(\omega_s t) \qquad (1)$$

where s represents the level of sympathetic activation. Sympathetic activity occurs on a slow time scale-altering heart rate over a long duration (2, 16, 17). Accordingly ω_s is assigned a small value, producing slow waves of more than 10 s duration.

It is generally accepted that low levels of sympathetic activity will result in slow oscillations of sympathetic nerve activity entrained to the vasomotor oscillations. However, as the level of sympathetic activity increases, these oscillations are damped and the fluctuations disappear such that under intense sympathetic drive, the heart rate becomes metronomic in its regularity. This damped effect can be achieved by taking $\omega_s \to 0$ or by reducing the coupling between the sympathetic oscillator and the sinus oscillator by taking $C_s \to 0$.

Parasympathetic respiratory oscillator. This oscillator is intended to represent short-term activity impinging on the sinus node via the parasympathetic nervous system. Respiratory oscillations affect both the sympathetic and parasympathetic nervous systems; however, because of the slow response time of

the sympathetic system, these rapid oscillations are mediated purely by the parasympathetic system (2, 16, 17). The effects of respiration are described by the parasympathetic respiratory oscillator (p), which is governed by *Eq. 2*,

$$p = \sin(\omega_p t) \qquad (2)$$

where p represents the level of parasympathetic respiratory activation. This oscillator has a value of ω_p larger than ω_s, typically at the modeled respiration frequency.

Sinus oscillator. The sinus node oscillator is based on the formulation of the well-known integral pulse frequency modulation (IPFM) model. It is a useful description of how cardiac events are modulated by autonomic nervous activity, and its suitability for modeling the sinus node has been discussed by a number of researchers (1, 3, 7). The IPFM model generates heartbeats by integrating an input signal until it reaches a preset threshold of unity. At this point, a pulse is produced and the integrator is reset to zero. See Fig. 3. The mathematical representation is given in *Eq. 3*.

$$1 = \int_{t_k}^{t_{k+1}} [HR + m(t)]dt$$

$$x(t) = \sum_{k=1}^{N} \delta(t - t_k) \qquad (3)$$

The signal $m(t)$ is the input signal representing autonomic activity, and t_k is the time of the kth R wave.
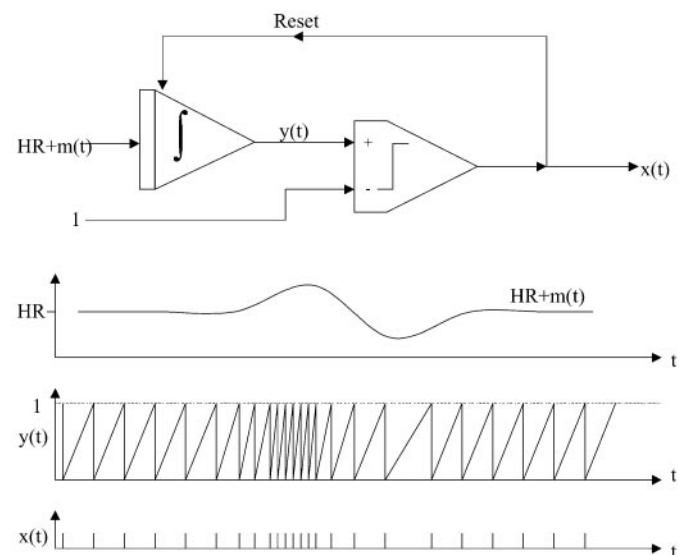

Fig. 3. Integral pulse frequency modulation (IPFM) model. Input signal $HR + m(t)$ is integrated until the integrator output $y(t)$ reaches the threshold of unity. At this point a pulse is produced in the output signal $x(t)$ and the integrator is reset.

When the input signal is zero, the IPFM model generates heartbeats with an interval equal to $\bar{I} = 1/HR$, where HR is a variable parameter that represents mean heart rate. It is equal to the actual frequency of heartbeats in the absence of any modulatory autonomic nervous activity. The input signal $m(t)$ represents the effects of modulatory autonomic nervous input and is defined by *Eq. 4*. If the input signal is positive, then heartbeats are generated at a faster rate, whereas a negative input signal causes heartbeats to be generated at a slower rate. The function $x(t)$ represents the series of pulses representing the heartbeats generated by the model, whereas $y(t)$ designates the integrator's output as a function of time.

We have formulated the modulation of the sinus oscillator by the sympathetic and parasympathetic oscillators as described by *Eq. 4*

$$m(t) = C_s s(t) + C_p p(t) \quad (4)$$

As a result, the sinus oscillator beats at a base rate of HR Hertz, which is increased or decreased in an additive linear fashion by sympathetic and parasympathetic respiratory modulation. For the modulating frequencies to appear unaliased in the beat sequence, the mean beat frequency HR should be higher than the highest modulating frequency component ω_p

$$HR \gg \frac{\omega_p}{2\pi} > \frac{\omega_s}{2\pi} \quad (5)$$

The coupling constants C_s and C_p reflect the levels of sympathetic and parasympathetic modulation of the sinus node, which is not equivalent to the tonic (mean) levels of sympathetic and parasympathetic activity. The tonic autonomic influences are included in the parameter HR, which is a combined function of sympathetic and parasympathetic activity, hormonal responses, and various parameters of the individual such as blood pressure. Accordingly HR is a function of the intrinsic heart rate HR_0 and the tonic influences of the autonomic system commonly referred to as the sympathovagal balance (5). Whereas the exact nature of sympathovagal balance is not completely understood, this concept has been formalized by the following model, $HR = HR_0 \times m \times n$, due to Rosenblueth and Simeone (16) and Katona et al. (11) in which $m > 1$ is the net sympathetic influence and $n < 1$ is the net parasympathetic influence. It is still being debated whether there exist any reliable connections between the tonic influences m and n and the levels of modulation C_s and C_p; however, it is often observed that heart rate and HRV are inversely related.

Accordingly, we model HR, C_s, and C_p as free variables so that it is possible to investigate sympathetic and parasympathetic interactions with C_s and C_p as functions of HR or sympathovagal balance. Note that C_s and C_p should be chosen such that $HR + m(t)$ is strictly positive.

CONVERGENCE BETWEEN MODEL AND ACTUAL HRV DATA

In this section, we demonstrate that our model displays the features of real R-R intervals under various induced autonomic balances. We consider the following conditions: complete autonomic blockade, parasympathetic blockade, and normal sympathetic-parasympathetic balance. Poincaré plots of the model's output are compared with plots of actual R-R intervals obtained from patients under the prescribed autonomic perturbations. The model's simulated autonomic balance is adjusted by varying the coupling constants, which alters the levels at which the oscillators influence the sinus oscillator. For all simulations, except where otherwise mentioned, the following constants were used

$$HR = 1.18 \text{ H}, \omega_s = 2\pi \times 0.025 \text{ rad/s},$$

$$\omega_p = 2\pi \times 0.344 \text{ rad/s} \quad (6)$$

HR corresponds to an R-R interval of 850 ms. The period of the sympathetic oscillator is set to ~40 s, and the parasympathetic oscillator is set to a period of ~3 s. Such a LF was used for the sympathetic oscillator, because it needs to account for the combined power of the LF and very low-frequency (VLF) bands to achieve a high degree of similarity between the plots from simulated and actual data.

Complete autonomic blockade. First, we consider the model's output in the absence of coupling, a state that is easily simulated with C_s and C_p taking on very small values. Consider Fig. 4*B* for which the coupling constants were $C_s = C_p = 0.01$. The Poincaré plot appears as a single dense point termed a "tight cluster." Because of the low coupling, there is very little variation in $m(t)$, and subsequently the sinus oscillator beats at a constant frequency of HR Hertz. Accordingly, the R-R intervals varied little from the constant value $1/HR$ seconds. The behavior of a denerved heart, such as found in the case of a transplant patient as in Fig. 4*A*, is mimicked. Figure 4*C* shows the power spectra of Fig. 4, *A* and *B*. It is seen that neither the transplant patient nor the model has any significant spectral power in either the LF or HF bands.

Unopposed sympathetic activity: parasympathetic blockade. This scenario is simulated by a high degree of coupling between the sympathetic oscillator and the sinus oscillator, whereas a low coupling level is used for the parasympathetic respiratory oscillator. Accordingly, the coupling constants take the values $C_s = 0.21$ and $C_p = 0$. The model's output, viewed as a Poincaré plot in Fig. 5*B*, is a slender closed loop oriented along the line $y = x$ and is suggestive of a "cigar" due to its shape. No variability is present other than the motion around the loop, a direct result of excluding the parasympathetic respiratory oscillator.

The plot in Fig. 5*A* is of a healthy subject who has been infused with atropine. The variability witnessed in this plot is therefore largely a product of sympathetic activity. The total lack of any short-term variability in our model's output prevents a clear comparison to this subject except at the most qualitative level.
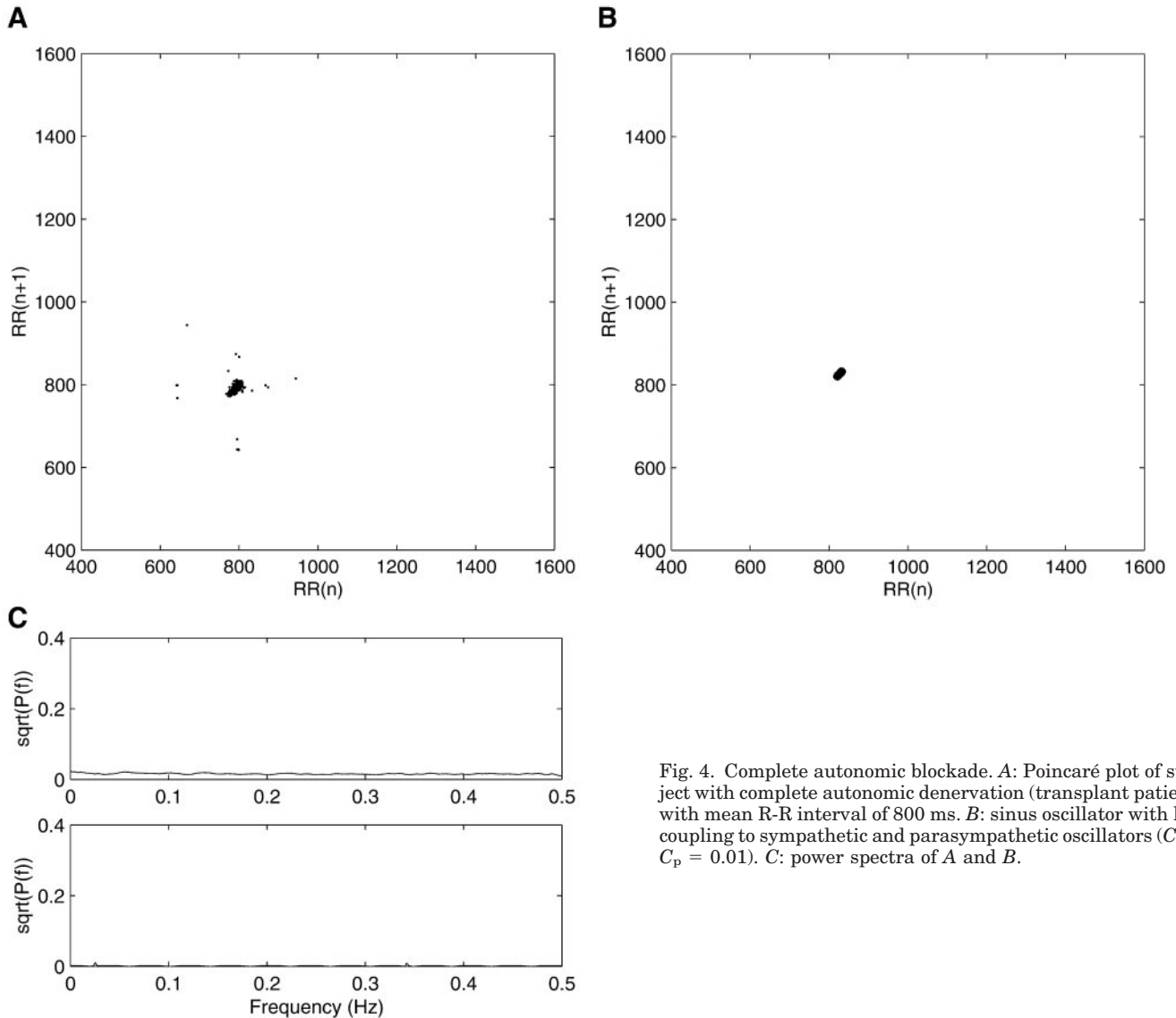
Fig. 4. Complete autonomic blockade. *A*: Poincaré plot of subject with complete autonomic denervation (transplant patient) with mean R-R interval of 800 ms. *B*: sinus oscillator with low coupling to sympathetic and parasympathetic oscillators ($C_s = C_p = 0.01$). *C*: power spectra of *A* and *B*.

Figure 5*C* shows the effect of artificially adding a small amount of short-term variability to the model's output by adding zero mean Gaussian noise with a standard deviation of 10 ms to the simulated intervals. A Poincaré plot very similar to actual observed cigar-shaped plots is observed. Real-life physiological systems usually do contain some level of spontaneous random variability that is best modeled as noise, particularly at this level. The model's output resembles R-R intervals recorded from patients with degraded parasympathetic nervous control, such as patients with heart failure (10). The length of the cigar is directly proportional to the amplitude of the sympathetic modulation of the sinus oscillator.

The power spectrum of the atropine-infused subject in Fig. 5*A* is shown in Fig. 5*D*, *top*. The spectrum is seen to consist of a substantial level of LF power and very little HF power. Figure 5*D*, *middle*, shows the power spectra of the model-generated R-R intervals.

The single peak in the LF band is the effect of the sympathetic oscillator with a coupling intensity of 0.21. Finally, Fig. 5*D*, *bottom*, shows the power spectrum of the model-generated R-R intervals with added noise. The noise adds a constant level across all frequencies to the power spectrum, and therefore, its presence does not overly alter the shape of the spectrum.

Sympathetic: parasympathetic balance. In this scenario, levels of parasympathetic respiratory activity are introduced. This is simulated by way of a small coupling intensity for the parasympathetic respiratory oscillator in addition to a high level of sympathetic coupling. Figure 6*B* shows the model's R-R interval output for the coupling constants $C_s = 0.3$ and $C_p = 0.05$. A large degree of variability emerges in the model's output in which the parasympathetic oscillator is responsible for the flanging effect or widening of the cigar shape into a "comet." Comparing Fig. 6, *A* and *B*, shows how closely the simulated R-R intervals resem-
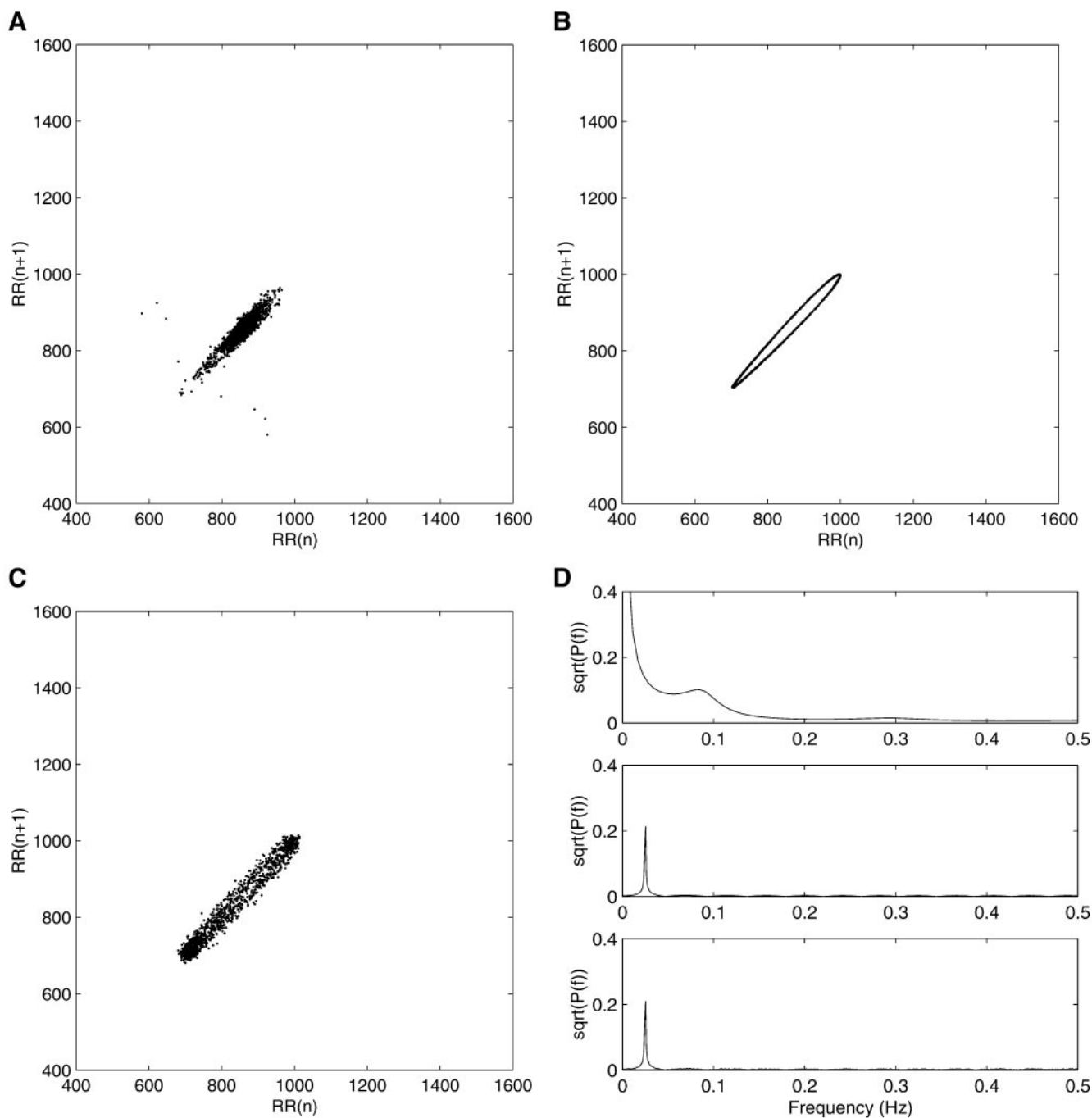
Fig. 5. *A*: Poincaré plot of a subject that has been given atropine to block parasympathetic activity. *B*: model-generated R-R intervals when the sympathetic oscillator is coupled ($C_s = 0.21$ and $C_p = 0$). *C*: additive Gaussian noise with a standard deviation of 10 ms. *D*: power spectra of *A* (*top*), *B* (*middle*), and *C* (*bottom*).

ble a Poincaré plot of a subject at rest breathing quietly in the supine position. Increasing the parasympathetic respiratory oscillator's coupling intensity increases the width of the comet and consequently the level of short-term variability in the R-R intervals. Figure 6*C* demonstrates this effect with C_p taking on the value of 0.1. The width of the comet is also dependent on the frequency of the parasympathetic oscillator in an intui-

tive manner: larger values of ω_p yield wider comets because short-term variability is increased.

The power spectrum of the supine subject of Fig. 6*A* is presented in Fig. 6*D*, *top*. A substantial level of both LF and HF power is displayed. Figure 6*D*, *middle*, shows the power spectrum of the model-generated R-R intervals. The two peaks produced by the sympathetic and the parasympathetic oscillators with coupling in-
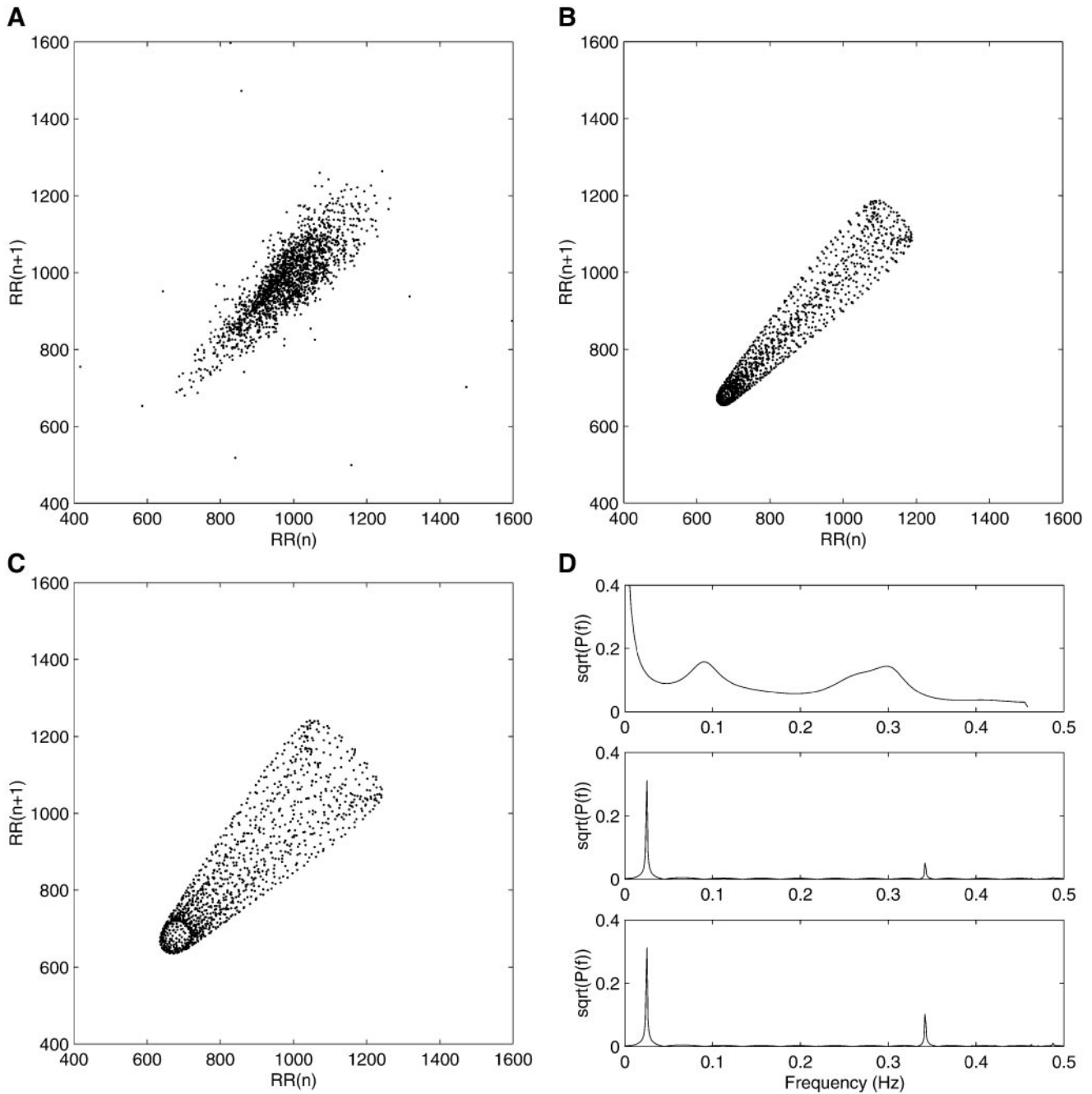
Fig. 6. Balanced sympathetic and parasympathetic activity. *A*: R-R intervals obtained from a subject who is lying supine and at rest. *B*: model's simulated output for the coupling constants $C_s = 0.3$ and $C_p = 0.05$. *C*: effect of increasing C_p to 0.1. *D*: power spectra of *A* (*top*), *B* (*middle*), and *C* (*bottom*).

tensities 0.3 and 0.05 are clearly shown. Figure 6*D*, *bottom*, displays the power spectrum of Fig. 6*C*, which has an increased value of 0.1 for the parasympathetic oscillator's coupling.

A significant difference exists between the Poincaré plots of the model-generated R-R intervals and the R-R intervals obtained clinically: the density of the points in the simulated cases are skewed toward the lower left corner of the plot, whereas actual R-R intervals are more

centrally distributed. The core of this discrepancy lies in the highly periodic nature of the oscillators. Fluctuations produced by the actual autonomic nervous system are not pure sinusoidal signals. Instead they resemble a random walk, which obtains low and high R-R interval lengths occasionally, while usually fluctuating about a mean value without deviating widely. It is important to observe that the lengths and widths of Fig. 6, *A* and *B*, are roughly the same. Our model shows it is this feature that

corresponds to the balance of LF and HF power being similar, not the dispersion of the points within the Poincaré plot.

MATHEMATICAL ANALYSIS OF HRV MODEL

This section develops a mathematical analysis used to investigate the length and width of the Poincaré plots generated from the HRV model developed in the previous sections. Because the model is a simplification of actual HRV mechanisms, these results will not apply to real HRV data in an exact sense. However, the results provide clear insight into the manner in which Poincaré plot descriptors vary as sympathetic and parasympathetic modulation levels are varied. Specifically, we characterize the theoretical dependency between LF and HF modulators and the shape of an R-R interval Poincaré plot generated by our model.

In accomplishing this analysis, we require an explicit solution to the R-R interval series. The remainder of this section derives this result. By defining the time of the initial beat to be the origin $t_0 = 0$, the defining equation for the IPFM oscillator (*Eq. 3*) can be expressed nonrecursively as

$$\int_0^{t_k} [HR + m(t)]\mathrm{d}t = k \quad (7)$$

where $m(t)$ is the modulating signal (3). In our model $m(t)$ consists of two frequency components. It turns out to be just as easy to work with N frequency components, so we consider $m(t) = \sum_{n=1}^{N} C_n \cos(\omega_n t + \phi_n)$ with $\omega_n < 2\pi HR$ for all n, i.e., slow modulation. The defining equation becomes

$$\int_0^{t_k} \left[1 + \bar{I} \sum_{n=1}^{N} C_n \cos(\omega_n t + \phi_n)\right]\mathrm{d}t = k\bar{I} \quad (8)$$

We have also divided through by HR and expressed $\bar{I} = 1/HR$ to make the equations simpler. After integration, the general relationship

$$t_k + \bar{I} \sum_{n=1}^{N} \frac{C_n}{\omega_n}[\sin(\omega_n t_k + \phi_n) - \sin(\phi_n)] = k\bar{I} \quad (9)$$

is obtained. Performing the substitution $t_k = k\bar{I} + \delta_k$, as per De Boer et al. (3), the following nonlinear relationship for δ_k is obtained

$$\delta_k = -\bar{I} \sum_{n=1}^{N} \frac{C_n}{\omega_n}[\sin(\omega_n k\bar{I} + \phi_n + \omega_n \delta_k) - \sin(\phi_n)] \quad (10)$$

The δ_k terms represent the amount each beat deviates from the regular pulse train $t_k = k\bar{I}$. *Equation 10* can be linearized about $\delta_k = 0$ provided $\omega_n \delta_k$ is small for all $n \in [1 . . N]$. If the event times are close to a regular pulse train ($\delta_k < \bar{I}/2\pi$) and the modulation frequencies are less than the mean beat frequency ($\omega_n < 2\pi HR$), it is obvious that $\omega_n \delta_k < 1$. Hence for a large class of practical pulse trains, including R-R intervals, a linear analysis is an accurate approximation. Linearizing about $\delta_k = 0$, we obtain

$$\delta_k = -\bar{I} \sum_{n=1}^{N} \frac{C_n}{\omega_n}[\sin(\omega_n k\bar{I} + \phi_n) - \sin(\phi_n) \\ + \omega_n \delta_k \cos(\omega_n k\bar{I} + \phi_n)] \quad (11)$$

Solving for δ_k gives the final expression for the beat times

$$t_k = k\bar{I} + \delta_k = k\bar{I} \\ + \frac{-\bar{I} \sum_{n=1}^{N} \frac{C_n}{\omega_n}[\sin(\omega_n k\bar{I} + \phi_n) - \sin(\phi_n)]}{1 - \bar{I} \sum_{n=1}^{N} C_n \cos(\omega_n k\bar{I} + \phi_n)} \quad (12)$$

The R-R intervals are $RR_k = t_{k+1} - t_k$. For our model, $N = 2$ and $C_1 = C_s$, $C_2 = C_p$, $\omega_1 = \omega_s$, $\omega_2 = \omega_p$ and $\phi_1 = \phi_2 = 0$. In this case, *Eq. 12* provides us with an accurate approximation to the R-R interval series generated by our HRV model. This result holds so long as the intervals are approximately regular and the modulation is slow. This is generally the case for R-R intervals. However, for subjects with very large HRV, the assumption that the intervals are approximately regular may be somewhat inaccurate. For the assumption $\delta_k < \bar{I}/2\pi$ to be compromised, an R-R interval would have to deviate from the mean R-R interval $\bar{I}$ by an amount greater than $\bar{I}/\pi \approx 0.32\bar{I}$.

Length of Poincaré plot main cloud. In this section we develop an approximation to the length of a Poincaré plot, depicted in Fig. 1B, as a function of the HRV model's coupling constants C_s and C_p. Researchers, who are dealing with noisy data, often employ the SDNN as a measure of Poincaré length (10, 19). For the purposes of this section, in which sequences lacking random variability are analyzed, it is simpler to define the length to be the distance between the extreme right- and left-most points of the Poincaré plot. The agreement between these two measures is a simple scaling by a constant. Thus length (L) is defined as the difference between the largest and smallest R-R intervals as shown.

$$L = \max_k RR_k - \min_k RR_k$$

Analytically deriving the maximum and minimum of the R-R interval series from *Eq. 12* is not straightforward; fortunately, these quantities can be approximated. By employing the standard approximation $(1 + z)^{-1} = 1 - z$ for $z < 1$, *Eq. 12* can be approximated as

$$\delta_k \approx \left\{-\bar{I} \sum_{n=1}^{N} C_n/\omega_n[\sin(\omega_n k\bar{I} + \phi_n) \\ - \sin(\phi_n)]\right\}[1 - \bar{I} \sum_{n=1}^{N} C_n \cos(\omega_n k\bar{I} + \phi_n)] \quad (13)$$

Expanding the brackets, combining sums, and using standard trigonometric identities, it is possible to express *Eq. 13* as a sum of sinusoids

$$\delta_k = -\bar{I} \sum_{n=1}^{N} \frac{C_n}{\omega_n} \{\sin [\omega_n k\bar{I} + \phi_n + \bar{I} \sum_{m=1}^{N} C_m \sin (\phi_m)]$$

$$- \sin (\phi_n)\} + \bar{I}^2 \sum_{n=1}^{N} \sum_{m=1}^{N} \frac{C_n C_m}{2\omega_n} \{\sin [(\omega_n - \omega_m)k\bar{I} + \phi_n$$

$$- \phi_m] + \sin [(\omega_n + \omega_m)k\bar{I} + \phi_n + \phi_m]\} \quad (14)$$

Hence, the R-R interval series, $RR_k = \bar{I} + \delta_k - \delta_{k-1}$, is

$$RR_k = \bar{I} - 2\bar{I} \sum_{n=1}^{N} \frac{C_n}{\omega_n} \sin \left[\frac{\omega_n \bar{I}}{2}\right] \cos \left[\omega_n k\bar{I} + \phi_n + \bar{I} \sum_{m=1}^{N} C_m \sin (\phi_m) - \frac{\omega_n \bar{I}}{2}\right]$$

$$+ \bar{I}^2 \sum_{n=1}^{N} \sum_{m=1}^{N} \frac{C_n C_m}{\omega_n} \left\{ \begin{array}{l} \sin \left[\frac{(\omega_n - \omega_m)\bar{I}}{2}\right] \cos \left[(\omega_n - \omega_n)k\bar{I} + (\phi_n - \phi_m) - \frac{(\omega_n - \omega_m)\bar{I}}{2}\right] \\ + \sin \left[\frac{(\omega_n + \omega_m)\bar{I}}{2}\right] \cos \left[(\omega_n + \omega_m)k\bar{I} + (\phi_n + \phi_m) - \frac{(\omega_n + \omega_m)\bar{I}}{2}\right] \end{array} \right\} \quad (15)$$

Assuming the maximum values of the time-varying sinusoids (those dependent on k) of *Eq. 15* are eventually sampled simultaneously at some point in time, an approximation to the upper limit of the length is obtained by replacing the sinusoids with the value 1. This approach gives the maximum length obtainable, a figure that is strictly an upper bound, yet also serves as an approximation to the true length L for modulation frequencies significantly less than the mean beat frequency. This is by virtue of having sampled frequently enough to examine arbitrarily close to the upper bound at some point in time. The upper bound on L is then twice the sum of the amplitudes of the frequency components described in *Eq. 15*. As $C_n < 1$, L is largely determined by the first-order terms. *Equation 16* is the first-order approximation to length. It is noted that this quantity is no longer the strict upper bound on L due to discarding the higher order contributions; however, it remains an approximation to the true length.

$$L \approx 4\bar{I} \sum_{n=1}^{N} \frac{C_n}{\omega_n} \left| \sin \left(\frac{\omega_n \bar{I}}{2}\right) \right| \quad (16)$$

Therefore, Poincaré plots obtained from our HRV model have a length approximated by

$$L \approx \frac{4}{HR} \left[\frac{C_s}{\omega_s} \left| \sin \left(\frac{\omega_s}{2HR}\right) \right| + \frac{C_p}{\omega_p} \left| \sin \left(\frac{\omega_p}{2HR}\right) \right| \right] \quad (17)$$

The actual (true) Poincaré plot length as a function of the HRV model's coupling constants C_s and C_p over the range 0.0–0.15 is shown in Fig. 8*A* (obtained via simulations). Length appears to be dependent on C_s and C_p in an almost identical manner and to behave linearly, in agreement with this analysis. Figure 8*C* compares true length to the approximation to length given by *Eq. 17*. For $C_s + C_p < 1$, the approximation is in excellent

agreement with the true length. As $C_s + C_p$ increases, second-order influences begin to become significant due to nonlinear effects becoming prominent, as expected from the analysis. The approximately identical manner that the coupling constants control the length can be explained by noting that $\sin(x) \approx x$ when $x < 1$ and for low modulation frequencies $\omega_p < 2\pi HR$. Accordingly, *Eq. 17* behaves as

$$L \approx \frac{2}{HR^2} (C_s + C_p) \quad (18)$$

These results state that HF and LF modulations affect L in equivalent manners for slow modulation and in a linear fashion for small coupling intensities. Under these conditions, length reflects neither the HF nor the LF modulations more significantly than the other. Thus, for practical purposes, length may be considered a measure of total modulation and is akin to the total power of the modulating signal.

Width of the Poincaré plot main cloud. The width of the main cloud of an R-R interval Poincaré plot characterizes the dispersion of points about the line of identity. Common measures of the width are the SDSD and the RMSSD of the R-R intervals (10, 19). As for the length of the model-based Poincaré plot, the lack of any
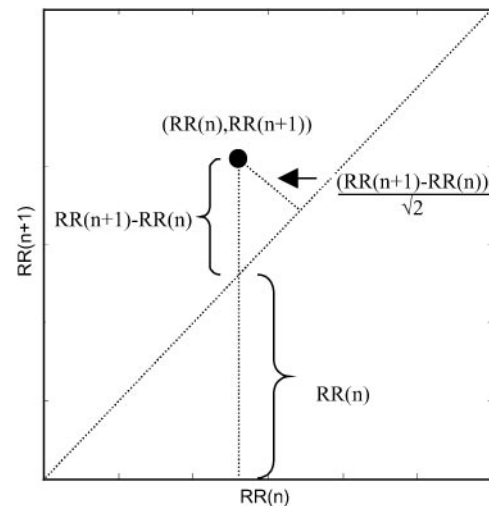

Fig. 7. Poincaré width, W, is measured as the largest difference between consecutive intervals, multiplied by the square root of 2. See text for additional information.

random component is exploited, and the width is defined to be the distance between the extremities as depicted in Fig. 1*B*. Thus the width is

$$W = \sqrt{2}\max_k |\Delta RR_k|$$

as Fig. 7 details. This expression involves the "delta" R-R intervals, $\Delta RR_k = RR_k - RR_{k-1}$, which are also known as the successive differences of the R-R intervals. They are given by

$$\Delta RR_k = -4\bar{I} \sum_{n=1}^{N} \frac{C_n}{\omega_n} \sin^2 \left(\frac{\omega_n \bar{I}}{2}\right) \sin \left(\omega_n k\bar{I} + \phi_n + \bar{I} \sum_{m=1}^{N} C_m \sin(\phi_m) - \omega_n \bar{I}\right)$$

$$+ 2\bar{I}^2 \sum_{n=1}^{N} \sum_{m=1}^{N} \frac{C_n C_m}{\omega_n} \left\{ \begin{array}{l} \sin^2 \left[\dfrac{(\omega_n - \omega_m)\bar{I}}{2}\right] \sin \left[(\omega_n - \omega_m)k\bar{I} + (\phi_n - \phi_m) - (\omega_n - \omega_m)\bar{I}\right] \\ + \sin^2 \left[\dfrac{(\omega_n + \omega_m)\bar{I}}{2}\right] \sin \left[(\omega_n + \omega_m)k\bar{I} + (\phi_n + \phi_m) - (\omega_n + \omega_m)\bar{I}\right] \end{array} \right\} \quad (19)$$

As can be seen from *Eq. 19*, the ΔRR intervals posses no direct current component, which is expected due to the zero average. Similar frequency content is present as for the length, except for being phase shifted and being multiplied by an extra $\sin(\cdot)$ term leading to the squared coefficient. An approximation to W is determined by taking an upper bound for W (by replacing the time-varying sinusoids with unity) and retaining only first-order terms as detailed in the calculations for length

$$W \approx 4\sqrt{2}\bar{I} \sum_{n=1}^{N} \frac{C_n}{\omega_n} \sin^2 \left(\frac{\omega_n \bar{I}}{2}\right) \quad (20)$$

For our HRV model, this expression is

$$W \approx \frac{4\sqrt{2}}{HR}\left[\frac{C_s}{\omega_s} \sin^2 \left(\frac{\omega_s}{2HR}\right) + \frac{C_p}{\omega_p} \sin^2 \left(\frac{\omega_p}{2HR}\right)\right] \quad (21)$$

Figure 8*B* details how true width varies as the coupling parameters are varied over the range 0.0–0.15. A comparison of *Eq. 21* to the true width is given in Fig. 8*D*. It is seen that the approximation to W is accurate when $C_s + C_p < 1$ but deviates widely as $C_s + C_p$ becomes large, due mainly to second-order influences becoming prominent. It can be seen from Fig. 8*B* that the level of HF modulation, C_p, is the dominant parameter controlling width. This property is clearly seen from the analysis, especially for small modulation frequencies ($\omega_s < 2\pi HR$) as *Eq. 21* behaves approximately as

$$W \approx \frac{1}{\sqrt{2}HR^3}(C_s\omega_s + C_p\omega_p) \quad (22)$$

Roughly speaking, the width of a Poincaré plot is a function of the weighted sum of the LF and HF amplitudes, where each amplitude is weighted by the respective angular frequency. Accordingly, HF components contribute to the width in larger amounts, and LF components contribute at minor, yet still significant levels. As will be explained later, Poincaré plot width should correlate highly with HF power and correlate at small levels with LF power.

Poincaré plot morphological properties for the HRV model. As the previous sections have shown, the correspondence between the HRV model's parameters and the Poincaré plot's shape can be accurately approximated by a linear transformation for small coupling intensities

$$\begin{bmatrix} L \\ W \end{bmatrix} = \begin{bmatrix} \dfrac{4}{HR\omega_s} \sin \left(\dfrac{\omega_s}{2HR}\right) & \dfrac{4}{HR\omega_p} \sin \left(\dfrac{\omega_p}{2HR}\right) \\ \dfrac{4\sqrt{2}}{HR\omega_s} \sin^2 \left(\dfrac{\omega_s}{2HR}\right) & \dfrac{4\sqrt{2}}{HR\omega_p} \sin^2 \left(\dfrac{\omega_p}{2HR}\right) \end{bmatrix} \begin{bmatrix} C_s \\ C_p \end{bmatrix} \quad (23)$$

The significance of this result is that the morphology of a Poincaré plot encodes the amplitudes of the modulation signal, allowing recovery of the amplitudes for signals composed of two known frequency components.

$$\begin{bmatrix} C_s \\ C_p \end{bmatrix} = \frac{1}{\gamma} \begin{bmatrix} \dfrac{\sin(\omega_p/2HR)\omega_s HR}{4\sin(\omega_s/2HR)} & \dfrac{-\sqrt{2}\omega_s HR}{8\sin(\omega_s/2HR)} \\ \dfrac{-\sin(\omega_s/2HR)\omega_p HR}{4\sin(\omega_p/2HR)} & \dfrac{\sqrt{2}\omega_p HR}{8\sin(\omega_p/2HR)} \end{bmatrix} \begin{bmatrix} L \\ W \end{bmatrix} \quad (24)$$

$$\gamma = \sin(\omega_p/2HR) - \sin(\omega_s/2HR)$$

For our model, it is theoretically possible to estimate similar characteristics to HRV spectral analysis, such as LF power, HF power, and HF/LF ratios, from the shape of the Poincaré plot by assigning appropriate values to the constants ω_s and ω_p. This is in addition to investigating the detailed beat-to-beat characteristics of HRV data. It should be noted that this property only applies exactly for modulation signals composed of only two frequency components. How well the correspondence generalizes to actual HRV data is dependent on how well the HRV spectrum is approximated by two dominant peaks.

GENERALIZATION TO REAL HRV DATA

At this point it is interesting to consider how well the results of the previous section apply to actual data obtained from subjects under various autonomic conditions. The results are not expected to apply com-
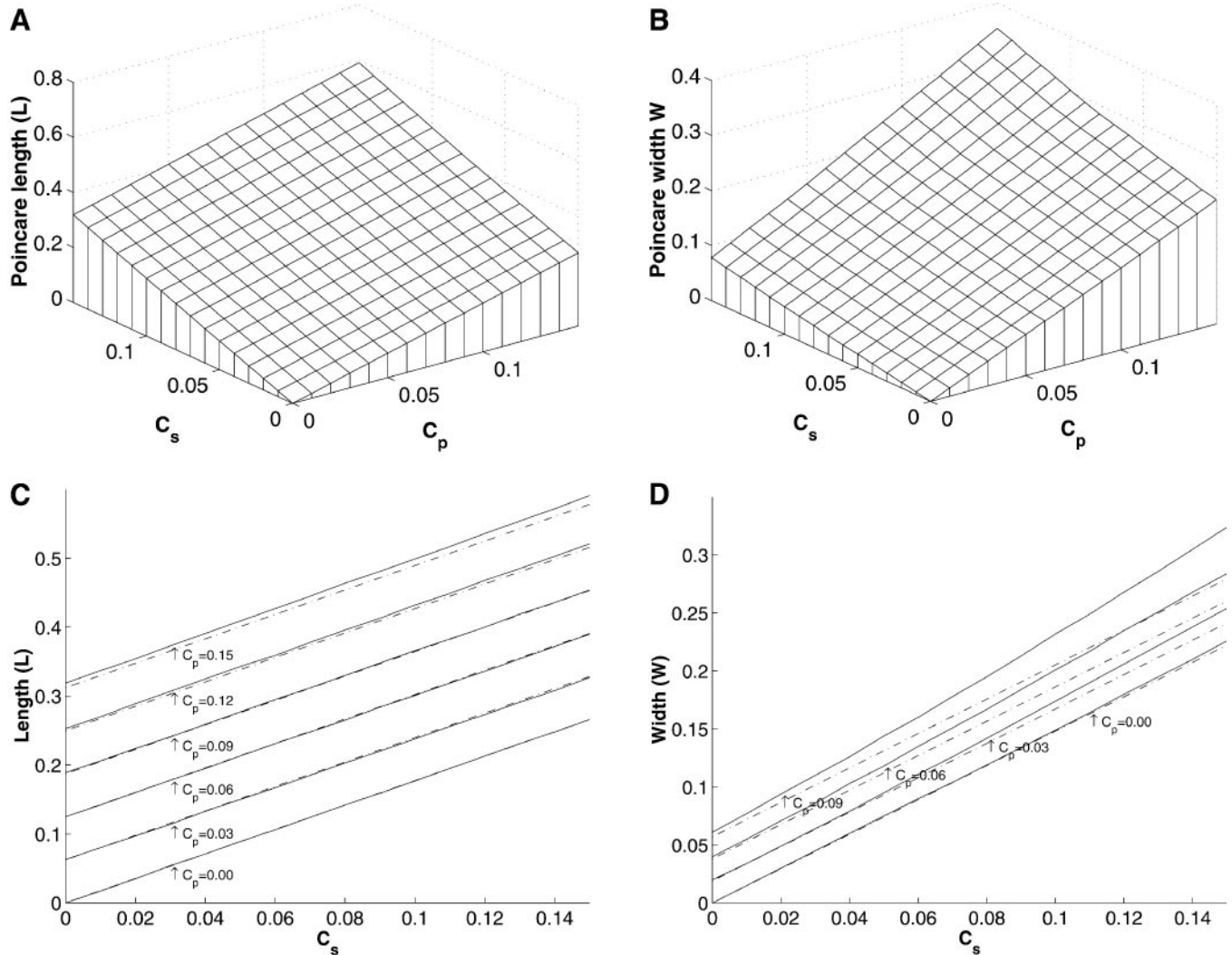
Fig. 8. Plots of width and length of Poincaré plot main clouds as the two coupling parameters are varied over the range 0.0–0.15. *A* and *B*: length and width, respectively, obtained from simulated R-R intervals. *C* and *D*: how analytic approximations to length (solid line compared with *Eq. 17*, dotted line) and width (solid line compared with *Eq. 12*, dotted line) compare.

pletely because they stem from a model of a discrete spectrum, but the principles identified by the analysis should be evident.

Data set acquisition. We employ the data set of a previous study (9) because it contains subjects over a wide range of autonomic conditions. The data set consists of 10 healthy subjects (5 female, 5 male) aged between 20 and 40 yr (30.2 ± 7.2 means ± SD). Each subject underwent four autonomic purtubations: *1)* baseline study with subjects in the supine position in a quiet environment; *2)* 70° head-up tilt, which increases sympathetic activity and decreases parasympathetic activity; *3)* atropine infusion, which markedly decreases parasympathetic nervous system activity; and *4)* transdermal scopolomine, which increases parasympathetic nervous activity. In all, 40 records were collected, each containing 1,024 R-R intervals.

Data set analysis. For each data set, the length and width of the Poincaré plot and the LF and HF power

were calculated. The length was calculated by $L = 2SDRR$, and the width by $W = \sqrt{2}SDSD$, as can be derived from simple geometry. The LF and HF parameters were calculated by using the autoagressive technique with the modified covariance technique (12). The bands were LF = 0.04–0.15 Hz and HF = 0.15–0.4 Hz. The length and width of the Poincaré plot were then derived from the LF and HF power by using *Eq. 23* with $C_s/HR^2 = \sqrt{LF}$ and $C_p/HR^2 = \sqrt{HF}$. The coupling constants need to be divided by *HR* twice, once as HRV spectral analysis techniques assume that the modulation signal in *Eq. 3* is dimensionless (1–3) and again as we need to multiply by the mean beat interval to normalize the discrete spectra units to those of the continuous spectrum (3). The derived length and width are compared with the actual length and width by plotting them against each other as scatterplot. The value of *HR* is calculated as the inverse of the average R-R interval. The choice of suitable values for ω_s and ω_p
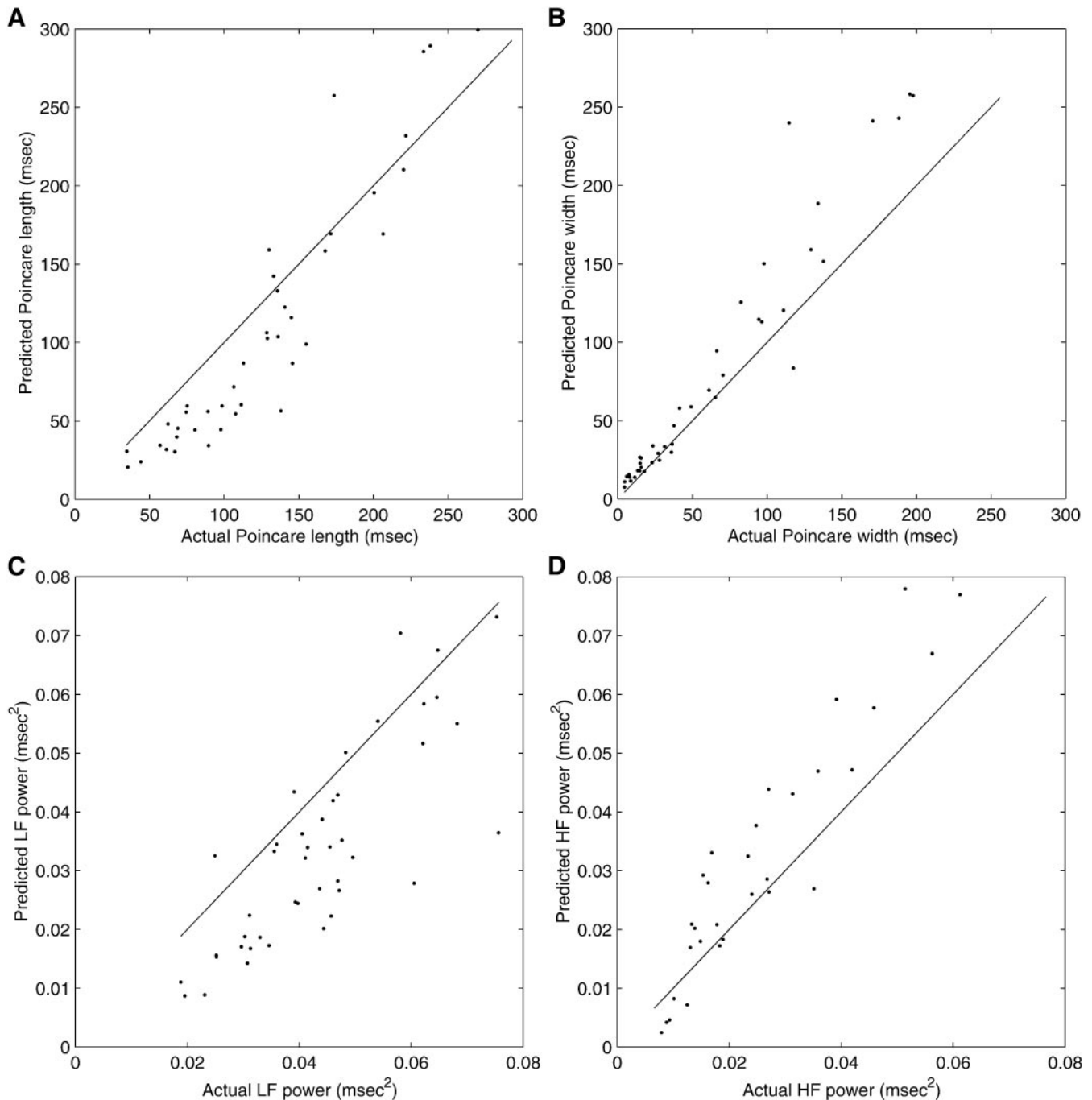
Fig. 9. Comparisons of derived parameters versus actual values. Correlation coefficients are 0.94 (*A*, length from LF and HF), 0.97 (*B*, width from LF and HF), 0.81 (*C*, LF from length and width), and 0.94 (*D*, HF from length and width).

is akin to the choice of the LF and HF bands. The midfrequencies of the bands is the most appropriate choice, i.e., $\omega_s = 2\pi(0.1)$ and $\omega_p = 2\pi(0.28)$ rad/s.

Figure 9*A* displays the derived length on the vertical axis and the actual length on the horizontal axis. The points do reflect the line of identity; however, there exists a fair amount of variability, which indicates that that *Eq. 23* does not hold entirely. The goodness of fit to the line of identity can be quantified by the correlation coefficient. Figure 9*A* has a correlation coefficient of

0.94, indicating that that *Eq. 23* holds reasonably well in determining the actual length. *Equation 23* has a tendency to underestimate the actual length, which is partially explained by noting that the length is a measure of all the modulation, yet LF and HF measure only the power from 0.04 Hz upwards, ignoring the VLF band. The derived width versus the actual width is plotted on Fig. 9*B*. A very good fit with a correlation coefficient of 0.97 occurs. The superior performance of *Eq. 23*, when predicting the width of a Poincaré plot,

can be explained by noting that ignoring the VLF power will not adversely affect the width as it is dominated by HF power.

The same analysis is now repeated for the reverse situation. Starting with the length and width of a Poincaré plot, we derive the LF and HF power by using *Eq. 24* with $\sqrt{LF} = C_s/HR^2$ and $\sqrt{HF} = C_p/HR^2$. The derived values of LF and HF are compared with the actual LF and HF values calculated by spectral analysis. Figure 9*C* displays the actual LF power versus the derived LF power. A correlation coefficient of 0.81 indicates a reasonable fit, and it is clear that the main trend of the relationship between LF power and length and width expressed by *Eq. 24* holds. Figure 9*D* compares derived HF power with actual HF power. A correlation coefficient of 0.93 indicates that *Eq. 24* explains the dependency of HF on the length and width very well.

These results clearly show that the principles identified from *Eqs. 23* and *24* are indeed present for actual HRV data. The fact that a discrete spectrum consisting of only two components can explain so much about the relationships among LF, HF, length, and width of a Poincaré plot is remarkable.

Poincaré plot morphology for real data. The results of the previous sections imply that the width is a measure of short-term variability and the length is a measure of total variability. This result has consequences for the correlations between frequency domain indexes and Poincaré plot indexes. Attempting to correlate LF power with Poincaré length (or equivalent SDNN measures) will explain only part of the variations in Poincaré length. Substantial portions of the variations are due to the codependency with HF power and will appear as uncorrelated noise. In data sets where significant variations in both LF and HF power are present, our model predicts that Poincaré length will correlate reasonably well with both LF and HF power; however, it will correlate highly with neither due to the variations introduced by the other. For Poincaré width, the dependencies on HF power are stronger than those of LF power. A strong correlation is expected when comparing HF power to Poincaré width, because the variations due to LF power will be small. LF power should correlate with Poincaré width, albeit at low levels, because LF power does influence the width, but the variations present due to HF power are large and reduce the correlation coefficient markedly.

Many of these results have already been shown experimentally. Specifically, our findings corroborate the findings of Otzenberger et al. (13), who found that SDNN (Poincaré length) correlated with both LF and HF power and RMSSD (Poincaré width) correlated with HF power and, to a lesser extent, LF power. Tullppo et al. (19), who investigated HRV and exercise, also present experimental results that agree: SDNN correlated almost equally with HF (Pearson's correlation coefficient: $r = 0.75$) and LF ($r = 0.72$) power, and RMSSD correlated highly with HF power ($r = 0.97$) and to a lesser yet significant extent with LF power ($r = 0.65$).

In conclusion, we develop a new mathematical model with a network of oscillators. For the first time, Poincaré plots are generated from the model and compared with Poincaré plots generated from subjects under various autonomic conditions. Now one can clearly understand how various autonomic regimes appear on the Poincaré plot through the use of the model.

Traditionally, researchers have identified length and width of Poincaré plots with LF and HF powers, respectively, of the HRV signal. However, with the use of our model, we establish that the length and width are not separately related but are a weighted combination of LF and HF power. This investigation provides a theoretical link between frequency domain spectral analysis techniques and time domain Poincaré plot analysis.

To determine the degree to which our results generalize to actual HRV data, we applied the model-based formulas to a set of clinical data. The results indicate that the formulas do identify clear trends in the relationships between the spectral components and Poincaré length and width. This gives definitive evidence that for HRV data, the length is a display of total modulation and the width indicates predominately short-term modulation. In summary, this study provides clear mathematical insight into the nature of observed data.

REFERENCES

1. **Berger RD, Askelrod S, Gordon D, and Cohen RJ.** An efficient algorithm for spectral analysis of heart rate variability. *IEEE Trans Biomed Eng* 33: 900–904, 1986.
2. **Berger RD, Saul JP, and Cohen RJ.** Transfer function analysis of autonomic regulation. I. canine atrial rate response. *Am J Physiol Heart Circ Physiol* 256: H142–H152, 1989.
3. **De Boer RW, Karemaker JM, and Strackee J.** Spectrum of a series of point events, generated by the integral pulse frequency modulation model. *Med Biol Eng Comput* 23: 138–142, 1985.
4. **De Meersman RE, Reisman SS, Daum M, Zorowitz R, Leifer M, and Findley T.** Influence of respiration on metabolic, hemodynamic, psycometric, and R-R interval power spectral parameters. *Am J Physiol Heart Circ Physiol* 269: H1437–H1440, 1995.
5. **Goldberger JL.** Sympathovagal balance: how should we measure it? *Am J Physiol Heart Circ Physiol* 276: H1273–H1280, 1999.
6. **Hojgaard MV, Holstein-Rathlou NH, Agner E, and Kanters JK.** Dynamics of spectral components of heart rate variability during changes in autonomic balance. *Am J Physiol Heart Circ Physiol* 275: H213–H219, 1998.
7. **Hyndman BW and Mohn RK.** A pulse modulator model of pacemaker activity (Abstract). *Digest of the 10th International Conference on Medicine and Biology Engineering.* Dresden, Germany: 1973, p. 223.
8. **Kamen PW.** Heart rate variability. *Aust Fam Physician* 25: 1087–1094, 1996.
9. **Kamen PW, Krum H, and Tonkin AM.** Poincaré plot of heart rate variability allows quantitative display of parasympathetic nervous activity. *Clin Sci (Lond)* 91: 201–208, 1996.
10. **Kamen PW and Tonkin AM.** Application of the Poincaré plot to heart rate variability: a new measure of functional status in heart failure. *Aust NZ J Med* 25: 18–26, 1995.
11. **Katona P, McLean M, Dighton D, and Guz A.** Sympathetic and parasympathetic cardiac control in athletes and non-athletes at rest. *J Appl Physiol* 52: 1652–1657, 1982.
12. **Mainardi LT, Bianchi AM, Baselli G, and Cerutti S.** Pole-tracking algorithms for the extraction of time-variant heart rate

variability spectral parameters. *IEEE Trans Biomed Eng* 42: 250–259, 1995.

13. **Otzenberger H, Gronfier C, Simon C, Charloux A, Ehrhart J, Piquard F, and Brandenberger G.** Dynamic heart rate variability: a tool for exploring sympathovagal balance continuously during sleep in men. *Am J Physiol Heart Circ Physiol* 275: H946–H950, 1998.

14. **Pomeranz B, Macaulay RJ, Caudill MA, Kutz I, Adam D, Gordon D, Kilborn KM, Barger AC, Shannon DC, Cohen RJ, and Benson H.** Assessment of autonomic function in humans by heart rate spectral analysis. *Am J Physiol Heart Circ Physiol* 248: H151–H153, 1985.

15. **Rompelman O, Snijders JBIM, and CJ van Spronsen.** The measurement of heart rate variability spectra with the help of a personal computer. *IEEE Trans Biomed Eng* 29: 503–510, 1982.

16. **Rosenblueth A and Simeone FA.** The interrelations of vagal and accelerator effects on the cardiac rate. *Am J Physiol* 110: 42–55, 1934.

17. **Sayers BM.** Analysis of heart rate variability. *Ergonomics* 16: 17–32, 1973.

18. **Sleight P, Rovere MTL, Mortara A, Pinna G, Maestri R, Leuzzi S, Bianchini B, Tavazzi L, and Bernard L.** Physiology and pathophysiology of heart rate and blood pressure variability in humans: is power spectral analysis largely an index of bararreflex gain? *Clin Sci (Lond)* 88: 103–109, 1995.

19. **Tulppo M, Makikallio TH, Takala TES, Seppanen T, and Kuikuri H.** Quantitative beat-to-beat analysis of heart rate dynamics during exercise. *Am J Physiol Heart Circ Physiol* 271: H244–H252, 1996.

20. **Warren JH, Jaffe RS, Wraa CE, and Stebbins CL.** Effect of autonomic blockade on power spectrum of heart rate variability during exercise. *Am J Physiol Regul Integr Comp Physiol* 273: R495–R502, 1997.

21. **Woo MA, Stevenson WG, Moser DK, and Middlekauff HR.** Complex heart rate variability and serum norepinephrine levels in patients with advanced heart failure. *J Am Coll Cardiol* 23: 565–591, 1994.

22. **Woo MA, Stevenson WG, Moser DK, Trelease RB, and Harper RH.** Patterns of beat-to-beat heart rate variability in advanced heart failure. *Am Heart J* 123: 704–710, 1992.